# A low complexity physics-based aging model for lithium ion cells with solid electrolyte interphase and lithium plating side-reactions

Alberto Romero<sup>1</sup> Elias Steinkellner<sup>1</sup> Johannes Angerer<sup>1</sup> Luca Belforte<sup>2</sup>

<sup>1</sup>Kreisel Electric, Austria, {alberto.romero, elias.steinkellner, johannes.angerer}@kreiselelectric.com

<sup>2</sup>Centro Ricerche FIAT (CRF), Italy, luca.belforte@crf.it

#### **Abstract**

In this paper, we extend our previously presented lithium ion battery model to include electrochemical aging dynamics, considering both calendaric and cyclic aging behavior. Accordingly, the Equivalent Hydraulic Model (EHM) is augmented with side reactions for Solid Electrolyte Interphase (SEI) growth and lithium plating. The model is validated against experimental results, showing a level of agreement that allows us to evaluate the effect of various charging and cooling strategies under realworld duty cycles. A case study concerning a battery electric passenger vehicle that operates under changing seasonal conditions illustrates the advantages of using such a model. Results show that the vehicle thermal management and the recharge strategy play a critical role in ensuring a long and safe operational life. In particular, and in agreement with the existing literature, more frequent charges that maintain a lower average state of charge, together with a lithium plating conscious thermal management, significantly extend battery lifetime.

Keywords: batteries, electrochemical model, aging, vehicle thermal management

#### 1 Introduction

The development and analysis of battery electric vehicles (BEVs) in the context of degradation presents multiple challenges. To begin with, the characterization of aging stress factors of commercial cells is a laborious and expensive task. Moreover, the real life operation of the battery packs, including the thermal management system (TMS) and battery management system (BMS), largely influence the way in which the individual cells of a battery pack will age.

Understanding the mechanisms by which the different functional components of a cell age is crucial. Safety can only be ensured if degradation is mitigated to the extent that batteries do not present hazardous behavior. Some relevant degradation mechanisms include: electrolyte decomposition, solid electrolyte interphase (SEI) growth and breakdown, gas evolution, overcharge, lithium plating, overdischarge, self-discharge, loss of active material, migration of soluble species, particle fracture, mechanical stress and structural changes (Arora, White, and Doyle

1998; Broussely 2002; Vetter et al. 2005; M. Broussely et al. 2005; Christensen and Newman 2006). Recent studies show that both SEI growth and lithium plating constitute the major drivers of aging under typical operating conditions (Ali et al. 2023; Che et al. 2023; Schlasza et al. 2014). Since battery degradation is caused by different stress factors, like high currents, extreme temperatures, or wide voltage windows, recommended limits have been developed to slow down or even avoid unnecessary damage (Fig. 1).

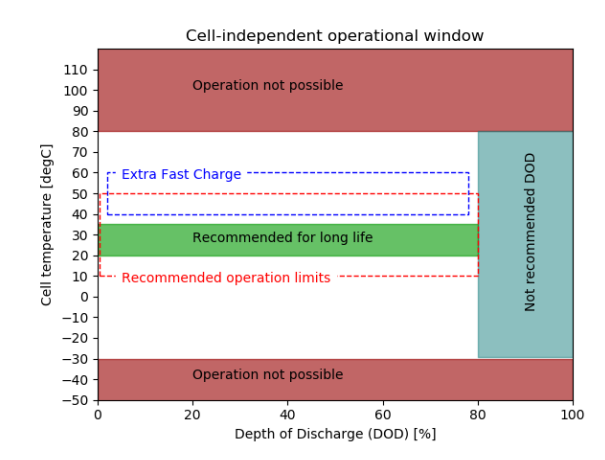


**Figure 1.** Summary of operational limits and recommendations for commonly used Li-ion cells (several sources)

Characterizing aging using mathematical expressions is needed to predict the likely degradation trajectory followed by the cell. Semi-empirical models have been proposed for this task as a default option because of its lower parametrization effort compared to physics-based models. The reader is referred to (Broussely et al. 2001; Ploehn, Ramadass, and White 2004; J. Wang et al. 2011; Rechkemmer et al. 2019) for different semi-empirical approaches. In general, however, these models can lump aging mechanisms unnecessarily, especially when more insight is needed in order to ensure a higher level of safety throughout the lifetime operation of the battery packs.

A novel physics-based aging model for Li-ion cells was described in (Yang, Leng, et al. 2017), that further enhances the electrochemical model previously developed by the authors (Gu and C. Wang 2000; Srinivasan and C.

Wang 2002). The aging model is based on the assumption that consumption of solvent and lithium plating (considered irreversible) contribute to the growth of the SEI layer, which in turns increases the film resistance and reduces the anode porosity. Since the aging model is applied on the socalled Newman's model (Marc Doyle, Fuller, and Newman 1993), the SEI growth and the appearance of lithium plating is spatially distributed. The model is reported to be effective capturing cyclic aging behavior observed experimentally. The approach is valid for the whole spectrum of C-rate and temperature when an Arrhenius dependency is added to the set of parameters (Yang and C.-Y. Wang 2018).

In a similar fashion (Li et al. 2019) adds an aging model on top of a reduced order electrochemical model, a further derivation of the Single Particle Model (SPM). This reduced order model assumes that the diffusion of lithium in the active material of the entire electrode can be represented by that of a characteristic spherical particle. The spatial gradient along the thickness of the electrodes, in the sense of concentration in solid and electrolyte phases, is therefore neglected. For a detailed description of the SPM and a discussion of the range of validity compared to the Newman's model, the reader is referred to (Chaturvedi et al. 2010).

Building upon these and more recent development in the area of Li-ion cells aging modeling, we have implemented a low complexity aging model that extends our previous reduced-order electrochemical mathematical description (Romero and Angerer 2023). The main feature of our contribution is the coupling of temperature sensitive aging dynamics, suitable for lithium plating side reactions in cyclic conditions (under load), together with calendaric (storage) degradation, all in a minimal implementation of the conservation laws in these kind of cells.

The remainder of the paper is organized as follows. First the electrochemical model with aging dynamics is presented. Next, we briefly describe the validation results for a particular cylindrical cell. A case study is subsequently introduced, and the result of the different operational alternatives analyzed. The last section is devoted to conclusions and future work.

#### 2 Physics-based aging model implementation

#### 2.1 **Equivalent Hydraulic Model**

The EHM has been used in the literature in order to capture electrochemical dynamics with the lowest mathematical complexity, in particular for control purposes (Romagnoli et al. 2017; Romero, Goldar, Couto, et al. 2019; Goldar et al. 2020). The previous application in the Modelica language was presented in (Romero, Goldar, and Garone 2019; Romero and Angerer 2023).

The EHM considers two electrochemical states, the bulk and surface concentration, in representative solid particles of the positive and negative electrodes. They are normalized with the maximum concentration ( $c_{s,max}$ ) and denoted by SOC (state of charge) and CSC (critical surface concentration) respectively. If we assume that the intercalation dynamics is significantly faster in one of the electrodes (e.g. the positive), the SOC and CSC can be assumed identical and a linear combination of the bulk SOC of the other one (the negative). This assumption is needed for observability reasons(i.e., if the internal states need to be estimated from measured voltage and applied current, as it is normally the case) and can be justified depending on the chemistry and electrode design (Couto, Schorsch, et al. 2016). The model considers current density as input  $(I = i/A_{cell})$ , where  $A_{cell}$  is the electrode area, and i the electrical current, positive if discharge), which allows us to describe the dynamics independent of the cell size.

$$\frac{d \operatorname{SOC}_{n}}{dt} = -\gamma I \tag{1}$$

$$\frac{d \operatorname{SOC}_{n}}{dt} = -\gamma I \tag{1}$$

$$\frac{d \operatorname{CSC}_{n}}{dt} = \frac{g}{\beta (1 - \beta)} \left( \operatorname{SOC}_{n} - \operatorname{CSC}_{n} \right) - \frac{\gamma}{1 - \beta} I \tag{2}$$

$$SOC_{p} = \rho SOC_{n} + \sigma \tag{3}$$

$$CSC_p = SOC_p \tag{4}$$

$$V = U_{\rm p} - U_{\rm n} + \eta_{\rm p} - \eta_{\rm n} - (R_{\rm cc} + \frac{R_{\rm film}}{a \, l_{\rm n}}) I \tag{5}$$

$$\eta_{p,n} = \frac{RT}{\alpha F} \sinh^{-1} \left( \frac{\theta_{p,n} I}{\sqrt{\text{CSC}_{p,n} (1 - \text{CSC}_{p,n})}} \right) \quad (6)$$

$$\begin{split} \gamma &= \frac{3}{R_{\rm s} \, a \, F \, l \, c_{\rm s,max}} \quad g = \frac{147}{20} \, \tau \quad \beta = \frac{7}{10} \\ \tau &= \frac{R_{\rm s}^2}{D} \qquad \qquad a = 3 \frac{\varepsilon}{R_{\rm s}} \qquad \theta = \frac{1}{2 \, a \, l \, r_{\rm eff} \, c_{\rm e0}^{1/2} \, c_{\rm s,max}} \end{split}$$

Equations 1-6, describe the dynamics of bulk and surface concentration, making use of lumped parameters  $\gamma$ , g,  $\tau$ , and  $\theta$ . They are used in the second-order Padé approximation (Couto, Schorsch, et al. 2016), and the overpotential  $\eta$  as defined in (Chaturvedi et al. 2010). The purpose of  $\rho$  and  $\sigma$  is to determine the static relationship between the state of charge of each electrode, which is a simplification of a more complex lithium dynamic balance. Their values (here -0.94 and 0.92 respectively) depend on the cell electrode design and formation process (Couto and Kinnaert 2018).

Open circuit voltages ( $U_{p,n}$ , dependent only on  $CSC_{p,n}$ ), overpotentials, and the internal resistances, are used to calculate the cell voltage. The previously so-called film resistance is now divided into pure ohmic losses (contact resistance, tabs and current collectors mainly,  $R_{cc}$ , and the SEI layer resistance  $R_{\text{film}}$ , time-dependent, which will be derived in the following section.

Exemplary parameters for a cylindrical 21700 Li-ion cell with a nominal capacity of 5 Ah are included in Table 1. Since the focus is on an EHM with fast dynamics

in the cathode, only anode parameters are included. The values provided are temperature or concentration independent, except for  $r_{\rm eff}$ , which is considered temperature dependent. The exact expression cannot be disclosed, but typically an Arrhenius relationship is used in the literature. Unlike our previous work, now the active material volume fraction ( $\varepsilon$ ) changes in time as the battery ages. Accordingly, this variation represents the so called Loss of Active Material (LAM), and the details will be explained in the next section. For this reason, we considered  $\varepsilon_0$  the initial value of the variable.

Table 1. Cell model parameters

Parameter	Units	Value
Electrode area, $A_{\text{cell}}$	$[m^2]$	0.1
Mass, $m_{\text{cell}}$	[kg]	0.07
Specific heat capacity, $C_{p,cell}$	[J/kg K]	800
Radial conductance, $G_{\text{rad}}$	[W/K]	1
Particle radius, $R_s$	$[\mu m]$	5
Electrode thickness, l	$[\mu m]$	80
Diffusion coefficient, D	$[m^2/s]$	1e-15
Active material vol. fraction, $\varepsilon_0$	%	75
Specific interfacial area, a	$[m^2/m^3]$	45e3
Effective reaction rate, $r_{\rm eff}$	$\left[\frac{A}{m^2}\left(\frac{m^3}{mol}\right)^{1.5}\right]$	7e-6
Maximum concentration $c_{s,max}$	$[\text{mol/m}^3]$	30e3
Electrolyte concentration, $c_{e0}$	$[mol/m^3]$	1200
Ohmic resistance, $R_{cc}$	$[m\Omega m^2]$	0.4

The thermal model assumes lumped properties concentrated on the cell core, typically the warmest region during normal operation. The thermal resistance consists of a serial summation of convection and conduction terms (external and internal heat flow respectively)

$$m_{\text{cell}} C_{\text{p,cell}} \frac{dT}{dt} = i \left( V - \left( U_{\text{p}} - U_{\text{n}} \right) + T \left( \frac{\partial U_{\text{p}}}{\partial T} - \frac{\partial U_{\text{n}}}{\partial T} \right) \right) - \frac{1}{R_{\text{th}}} \left( T - T_{\text{amb}} \right)$$

$$(7)$$

$$A = \pi D H_{\rm c} \quad R_{\rm th} = (\frac{1}{4 \pi H_{\rm c} k} + \frac{\ln(D_{\rm can}/D))}{2 \pi H_{\rm c} k_{\rm can}} + \frac{1}{hA})$$

where  $R_{\rm th}$  is the thermal resistance of the lumped thermal model of the cell, h is the heat transfer coefficient w.r.t. the cooled/heated section, and  $\frac{\partial U_{\rm p(n)}}{\partial T}$  define the so called entropic heat of the positive (negative) electrode (Dao and Schmitke 2015). We note here that this model approximates the behavior of an infinite cylinder with homogeneous heat generation. In reality, the active cooling/heating area is limited to a portion of the total height of the cell (assuming side cooling), while the rest is cooled passively by natural convection typically with the surrounding air. The cell housing conductivity is high enough, and its thickness sufficiently small, to neglect its

contribution in the total resistance. The core to surface conductance in radial direction can be simplified as  $G_{\rm rad}$ . The entropic heat, as well as the heat transfer to the air, can also considered to be negligible. Thus, the simplified model can be reduced to

$$m_{\text{cell}} C_{\text{p,cell}} \frac{dT}{dt} = i (V - (U_{\text{p}} - U_{\text{n}})) - UA (T - T_{\text{amb}}), (8)$$

where U is the so called overall heat transfer coefficient, which includes internal conductance and external convection terms.

### 2.2 Aging model

 The extension of the electrochemical model is based on the work of (Yang, Leng, et al. 2017). Our adaptation considers the main assumptions:

- 1. Main aging mechanisms are surface film (SEI) growth, irreversible lithium plating, and loss of active material
- 2. Negligible aging in cathode material
- 3. Homogeneous degradation throughout the electrode volume.

The first two assumptions are compatible with the model described in (Yang, Leng, et al. 2017), and the last one is required by the nature of the EHM. In their work, two states are needed to define the accumulated aging, namely the reacted ethylene-carbonate to form new SEI ( $c_{\rm SEI}$ ) and the lithium plated ( $c_{\rm Li}$ ). This accumulation in the form of molar concentrations (per unit volume of the electrode) can be represented in the following differential equations

$$\frac{dc_{\text{SEI}}}{dt} = -\frac{j_{\text{SEI}}}{2F} - \frac{j_{\text{lpl}}}{F}\chi\tag{9}$$

$$\frac{dc_{\text{Li}}}{dt} = -\frac{j_{\text{lpl}}}{F}(1 - \chi). \tag{10}$$

where  $\chi$  is considered null as in the referenced work for simplicity. These two products form the so called SEI layer, a surface film whose thickness is proportional to their accumulation around the surface of the active material particles, or in mathematical form,

$$\delta_{\text{film}} = \frac{1}{a} \left( \frac{c_{\text{SEI}} M_{\text{SEI}}}{\rho_{\text{SEI}}} + \frac{c_{\text{Li}} M_{\text{Li}}}{\rho_{\text{Li}}} \right), \tag{11}$$

where  $M_{\rm SEI(Li)}$  and  $\rho_{\rm SEI(Li)}$  are the molar weight and density of each aging products. The thickness of the SEI layer defines in turns its resulting ionic resistance

$$R_{\text{film}} = \omega_{\text{SEI}} \frac{\delta_{\text{film}}}{K_{\text{SEI}}},$$
 (12)

with  $\omega_{\rm SEI}$ ,  $K_{\rm SEI}$  being the volume fraction of SEI in the film and the ionic conductivity respectively.

At this point, we introduce the alternative approach with respect to the work of (Yang, Leng, et al. 2017). Instead of assuming that the drop in porosity dominates the aging behavior, caused by the clogging of the void fraction by the SEI growth, we focus on the loss of active material degradation mechanism. Since the EHM neglects the transport dynamics in the electrolyte, it is not directly affected by changes in porosity. In contrast, one could associate the SEI buildup to the progressive isolation of active material regions, causing an apparent loss of active material (aLAM). This approach is similar to that found in (Li et al. 2019), originally proposed by (Fu et al. 2015). Accordingly, we can define the loss of active material as the decrease in active material volume fraction ( $\varepsilon$ )

$$\frac{d\varepsilon}{dt} = -a\frac{d\delta_{\text{film}}}{dt},\tag{13}$$

where it is explicit that the volume loss of accessible active material is proportional to the SEI volume increase. Equation 13 constitutes the derivative of the third aging state variable. This approach is similar to that followed by MapleSim's Battery Component Library (MapleSoft 2025), where the normalized remaining capacity depends on a cubic function of the SEI thickness. Therefore, our solution is a compromise between empirical simplicity and physical fidelity.

SEI growth is dominated by the concentration of ethylene-carbonate in the SEI layer and its thickness. The expressions found in (Yang, Leng, et al. 2017) were found to be suitable for our model in predicting cyclic aging, the original purpose of the model, but not calendaric aging. Therefore, a modified version of their work is presented here.

The volumetric current density associated to the SEI side reaction can be expressed as:

$$j_{\text{SEI}} = -aF k_{0,\text{SEI}} c_{\text{EC}}^{\text{s}}$$

$$\exp\left(-\frac{\alpha_{\text{c,SEI}} F}{RT} \left(\phi_{\text{s}} - \phi_{\text{e}} - \frac{j_{\text{tot}}}{a} R_{\text{film}} - U_{\text{SEI}}\right)\right)$$
(14)

where  $j_{\text{tot}}$  is the current density,  $k_{0,\text{SEI}}$  the reaction constant, and  $c_{\text{EC}}^{\text{s}}$  is the concentration of EC (ethylene carbonate) on the surface of the graphite (Yang, Leng, et al. 2017) or, more precisely, in the SEI layer (Zhao, Choe, and Kee 2018). According to the former, the solvent concentration can be computed with the following algebraic equation

$$-D_{\rm EC}\frac{c_{\rm EC}^{s} - c_{\rm EC}^{0}}{\delta_{film}} = -\frac{j_{\rm SEI}}{F}$$
 (15)

which neglects the time dependency of the diffusion process.

The diffusion of EC is considered to be enhanced with temperature, as remarked by (Zhao, Choe, and Kee 2018) following the Arrhenius form

$$D_{\rm EC} = D_{\rm EC,0} \exp\left(\frac{E_{\rm a}}{R} \left(\frac{1}{T} - \frac{1}{T_{\rm ref}}\right)\right). \tag{16}$$

Most studies on physics-based aging models focus on cyclic aging, where these are fitted to match experimental results under cyclic loading. Research shows (Jin and Liu 2019) that it is possible to derive the calendaric aging based on the concentration of products and reactants in the SEI layer, an approach which may lead to a better performance of the model, both for cyclic and calendaric aging. We have opted for a hybrid approach, where the diffusion of EC during storage conditions depends on the state of charge and the temperature

$$D_{\rm EC} = k_{\rm cal} D_{\rm EC,0} \, \text{SOC} \, \exp\left(\frac{-E_{\rm a}}{R} \left(\frac{1}{T} - \frac{1}{T_{\rm ref}}\right)\right), \quad (17)$$

where  $k_{\rm cal}$  limits the increase of calendaric aging as the SOC tends to 100% compared with the cyclic aging. The proportionality with SOC allows to also increase the observed impact of high SOC storage, which may not be captured completely in Eq.(14). This expression has been developed to mimic the behavior of the calendaric aging of the cell considered, but adjustments for alternative chemistries are possible.

Lithium plating is a phenomenon that tends to take place in the interface between anode and separator, and the last assumption is only justified because the aim of the aging model is mainly to capture the cycle or point in time when lithium plating starts occurring. As indicated in the literature (Yang, Leng, et al. 2017), as the SEI grows, the likelihood of plating increases. Therefore, a charging cycle that does not trigger lithium plating in a fresh cell, may do so after certain time in operation. It will be shown, nonetheless, that a model with homogeneous lithium plating captures the capacity loss when it takes place reasonably well, causing the rapid deterioration of the electrode. According to (Yang, Leng, et al. 2017), the side reaction current associated to lithium plating can be formulated as

$$j_{\rm lpl} = -a i_{0,\rm lpl} \exp\left(-\frac{\alpha_{\rm c,lpl} F}{RT} \left(\phi_{\rm s} - \phi_{\rm e} - \frac{j_{\rm tot}}{a} R_{\rm film} - U_{\rm lpl}\right)\right)$$
(18)

where  $i_{0,lpl}$  is the exchange current density of the lithium plating reaction. It should be noted that this side-reaction is active if the anode potential drops below the Li/Li<sup>+</sup> equilibrium potential ( $U_{lpl}$ ), and zero otherwise.

These equations and similar ones have been applied to electrochemical models of Li-ion cells, including SPM (Li et al. 2019). Since the EHM assumes constant electrolyte concentration, and it is therefore not modeled, the overpotential of reactions necessary to calculate the side reaction currents are expressed as follows:

$$\eta_{\text{SEI}} = \phi_{\text{s}}^{-} - \phi_{\text{e}}^{-} + \frac{j_{\text{tot}}}{a^{-}} R_{\text{film}} - U_{\text{SEI}} =$$

$$\eta^{-} + U^{-}(C_{\text{ss}}^{-}) - U_{\text{SEI}} \tag{19}$$

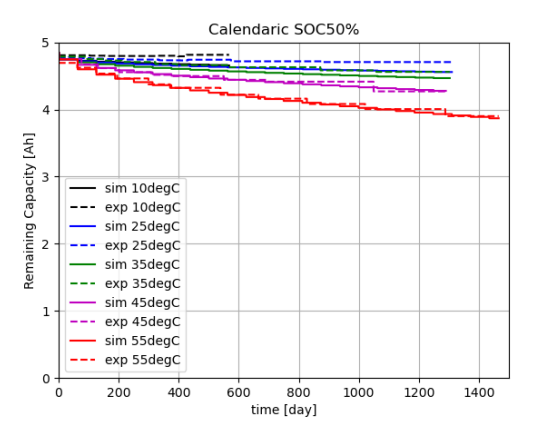
$$\eta_{\rm lpl} = \phi_{\rm s}^{-} - \phi_{\rm e}^{-} + \frac{j_{\rm tot}}{a^{-}} R_{\rm film} - U_{\rm lpl} = 
\eta^{-} + U^{-}(C_{\rm ss}^{-}) - U_{\rm lpl}$$
(20)

In order to avoid side reactions, the overpotential of the considered side reaction should always be non-negative:

$$\eta_{SR} = \eta + U(CSC) - U_{SR} \ge 0. \tag{21}$$

Table 2. Aging model parameters

Parameter	Units	Value
SEI growth reaction		
EC content in electrolyte, $c_{\rm EC,0}$	$[mol/m^2]$	4.5e3
Diffusion of EC, $D_{EC}$	$[m^2/s]$	2e-15
Conductivity, $\kappa_{\rm SEI}$	[S/m]	5e-6
Volume fraction, $\Omega_{SEI}$	[-]	0.01
Activation energy, $E_a$	[J/mol]	1e4
Kinetic rate constant, $k_{0,SEI}$	[m/s]	1e-12
Transport coefficient, $\alpha_{c,SEI}$	[kg/m <sup>3</sup> ]	0.5
Molar mass, $M_{\rm SEI}$	[kg/mol]	0.162
Density, $\rho_{\rm SEI}$	$[kg/m^3]$	1690
Side reaction eq. potential, $U_{\rm SEI}$	[V]	0.4
Lithium plating reaction		
Exchange current density, $i_{0,lpl}$	$[A/m^2]$	1e-3
Transport coefficient, $\alpha_{\rm c,lpl}$	$[kg/m^3]$	0.5
Molar mass, $M_{\rm Li}$	[kg/mol]	6.9e-3
Density, $\rho_{\rm Li}$	$[kg/m^3]$	534
Side reaction eq. potential, $U_{\rm lpl}$	[V]	0



(a) 50% SOC

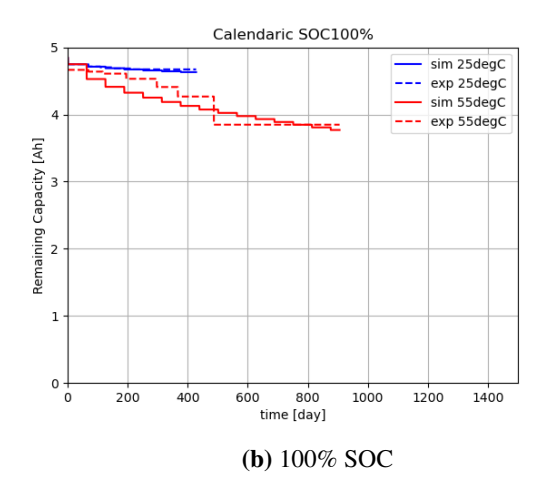
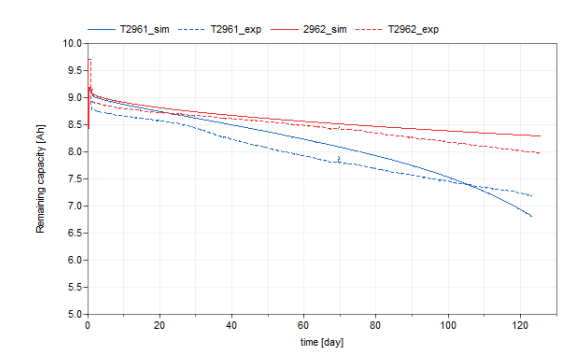


Figure 2. Calendaric aging validation results

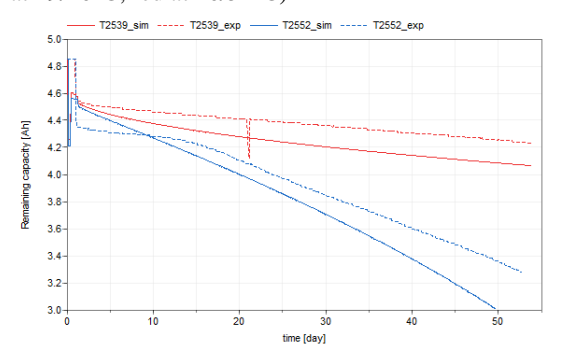
#### 3 Model calibration

In the first place, the chemistry and the main parameters of the electrochemical model were determined. The cathode composition is high-niquel NMC, and the anode contains mainly graphite as active material, as external laboratory analysis indicate. The total capacity is 5 Ah approximately, and the format is the conventional cylindrical 21700 (21 mm diameter, 70 mm height). Parameters concerning geometry (electrode area and thickness, particle diameter) and weight where measured either inhouse or by an external laboratory. The active material fraction was adjusted from a reference value borrowed from the literature (Chen et al. 2020). Thermal behavior  $(C_{p,cell}, G_{rad})$  could be adjusted from a large variety of input-output data from experimental tests under different boundary conditions (free convection at room temperature, controlled temperature chambers with forced air flow, and immersion cooling). The pure ohmic resistance was determined from ACIR (Alternating Current Internal Resistance at high frequency). Diffusion coefficients in the solid phase, as well as the remaining electrochemical properties (including  $U_{p,n}$ ) were adjusted from different literature sources or external laboratories. Values reported in Table 1 must be taken as exemplary, since the actual values are are kept confidential.

The required cyclic and calendaric aging tests have been conducted in-house to adjust the parameters of the aging model. Exemplary values are given in Table 2 since the actual ones cannot be disclosed. In addition, literature data and sensitivity analyses have been used to best characterize the cyclic and calendaric aging behavior. More specifically,  $U_{\rm SEI}$  is taken from (Zhao, Choe, and Kee 2018), while the remaining parameters were taken directly from (Yang, Leng, et al. 2017), or adapted from this source (mainly  $D_{\rm EC}$ ,  $\Omega_{\rm SEI}$ ). The activation energy was directly fitted from experimental data. Different temperature and SOC storage conditions were used in the storage tests (Fig. 2), while different current and temperature values were used under cycling, with emphasis on the corner cases where lithium plating was observed (Fig. 3). The observation involved a non-linear, accelerated capacity drop, as well as post mortem tear-down examinations. In particular, tests with CCCV charges 0.7C and 1C were chosen at temperatures below which, according to the manufacturer, lithium plating may occur (25°C and 35°C respectively).



(a) 0.7C charge / 1.5C discharge (two parallel cells, blue at 19/26°C, red at 26/31°C)



**(b)** 1C charge / 1.5C discharge (one single cell, blue at 22°C, red at 40°C)

**Figure 3.** Cyclic aging validation results at temperatures below and above the lithium plating recommended temperature

## 4 Case study

In order to highlight the benefits of the model presented above, we conducted a set of tests with varying operating conditions that affect the rates of calendaric and cyclic aging. The target cell corresponds to cylindrical cell similar to that described in previous sections. The full description of the pack, which uses immersion cooling in direct contact with the cells can be found in (Romero and Angerer 2023). Its size (60 kWh) is similar to that of a pack for mid-size battery electric vehicles. Only the behavior of a single cell is analyzed here, as though all cells would operate under the same boundary conditions. In reality, the resulting temperature spread within the pack will lead to heterogeneous aging, but this is out of the scope of this work.

All models described in this paper have been implemented in Dymola, but compatibility with other Modelica tools, i.e., OpenModelica, was ensured. Before describing the boundary conditions and the case study, we introduce two key components included in the case study simulation template.

#### 4.1 Thermal control

Electric vehicles use a sophisticated thermal management system, with control algorithms set to ensure an optimal operating temperature window. In our application, we define a hysteresis loop with immersion cooling (ON: 30°C,

OFF:25°C) and heating (ON: 10°C, OFF:15°C) that ensures practical operational temperatures. Sufficient thermal power is assumed, with a fixed temperature source of 30°C when heating and 25°C when cooling. In addition to the active cooling boundary, the cell model is thermally connected to the environmental temperature. The active thermal management guarantees around 100 W/m²K of heat transfer. A convective overall heat transfer coefficient to the ambient of 1 W/m²K is assumed. Both values have been experimentally determined for the pack considered where the cells are installed, and approximate values are reported.

#### 4.2 Cycler

Modelica classes have been developed to automate, in a virtual environment, the classical laboratory performance and cyclic aging. This includes lifetime simulations, where a rich set of mixed protocols are linked sequentially. This includes, e.g., CCCV charges and discharges, duty cycles, capacity check cycles, and DCIR tests. The ModelicaStateGraph2 library (Otter, Årzén, and Dressler 2005) is used to control the cycler states, but the building philosophy could be adapted to other similar libraries. An example of a custom cycler with profile input during the discharge state (without opportunity charge) is shown in Fig. 4. It must be noted that current, voltage or power are assigned in the equation section in the text layer (not shown here). The cycler variant used assumes eight different states or steps:

- 1. Initial step
- 2. Pre-charge
- 3. Constant current charge
- 4. Constant voltage charge
- 5. Idle time after charge
- 6. Pre-discharge
- 7. Duty-cycle
- 8. Pre-opportunity charge
- 9. Opportunity charge
- 10. Idle time after discharge.

Every day, a number of duty-cycles are repeated before and after a mid-day break, which considers a typical daily commute, including weekend leisure usage. Charging is allowed during nights of certain days (Wednesday, Saturday and Sunday) at a C-rate of 0.1C (w.r.t. nominal energy, 18 Wh), but opportunity charging below certain voltage is also possible (0.7C w.r.t. nominal capacity, 5 Ah). The effect on aging of these two charging possibilities is compared below.

The automotive driving profile was provided by Centro Ricerche FIAT (CRF) at cell level. The final power was re-scaled for an equivalent battery size of 50 kWh. The profile represents a typical WLTC with a duration of approximately 23 km and 1800 s. In the first option (light usage), we consider it is repeated once (1xWLTC) in the morning and once in the afternoon. In a second option (moderate usage), we increase to 2xWLTC, morning and

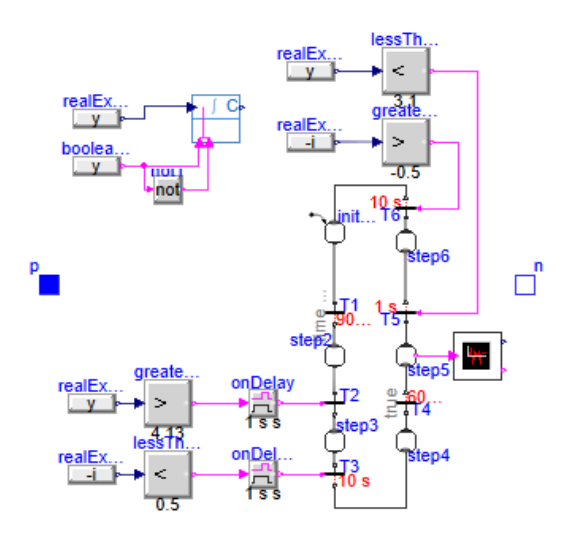


**Figure 4.** Simple cycler with power profile discharge using ModelicaStateGraph2

afternoon. Each of these options relate to vehicles driving around 150 and 300 thousand kilometers within ten years respectively.

#### 4.3 Additional boundary conditions

Two locations are considered in our study, namely Seville and Gothenburg. They present two extreme climatic options, represented by their ambient temperature (Fig. 5).

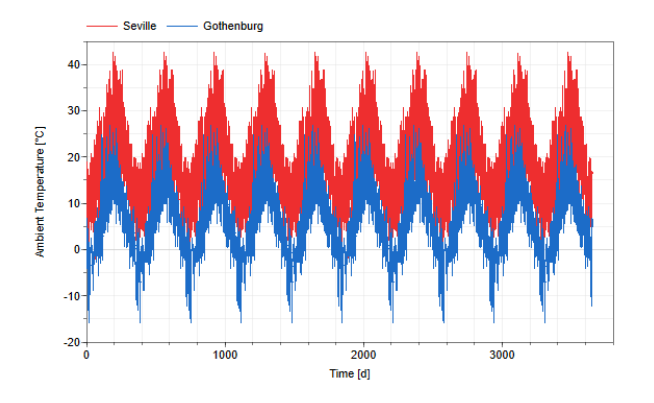


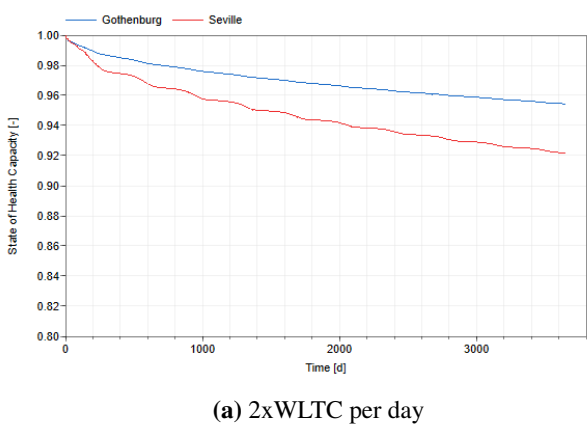
**Figure 5.** Local ambient temperatures (dry-bulb). Source https://pvwatts.nrel.gov/

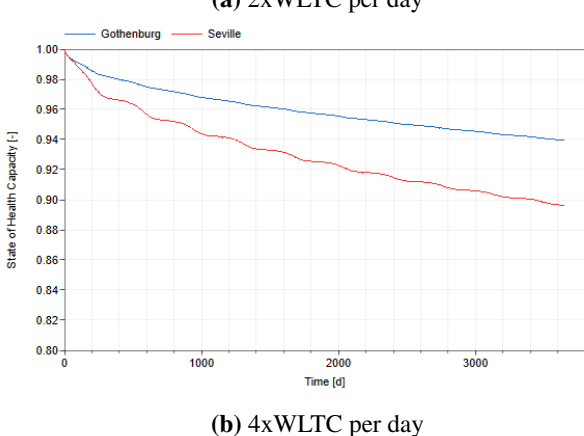
#### 5 Results

#### 5.1 Night charge

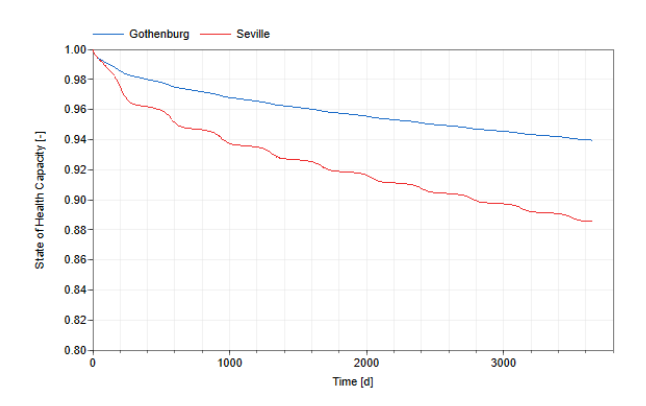
We first compare different levels of usage of the battery in Seville and Gothenburg for the night charge condition. Results are shown in Fig. 6 including light and moderate usage and default thermal management, as well as moderate usage and higher temperature cooling.

Figure 7 present results for simulations where thermal control for cooling is limited to an hysteresis loop between 40°C (ON) and 35°C(OFF). This setup affects mainly Seville, since Gothenburg's temperatures seldom reach 35°C.





**Figure 6.** Comparison between the effect of number of cycles per day and ambient temperature



**Figure 7.** 4xWLTC per day, two locations, higher cooling temperatures

For the case in which the lower temperature is not sufficiently limited by the battery heater (i.e., hysteresis setup 5°C(ON), 10°C(OFF)), the battery may charge or regenerate energy in conditions close to lithium plating. We have also considered the fact that the thermal management is not active during the idling period, which exacerbates the impact of low temperatures (Fig. 8).

For comparison, Fig. 9 illustrates the effect of each charging strategy on the voltage during two consecutive weeks. It can be seen that in both cases the anode potential drops below the lithium plating threshold.

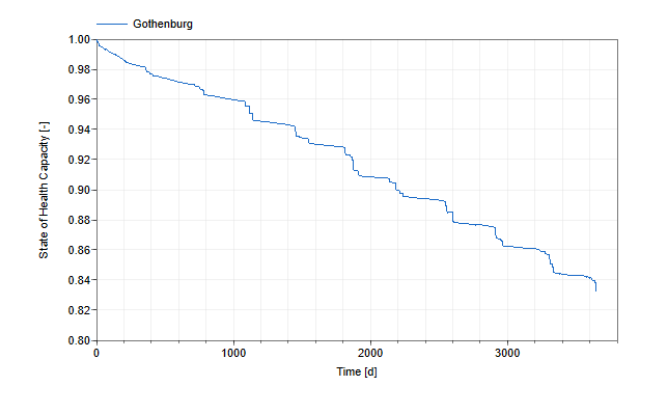
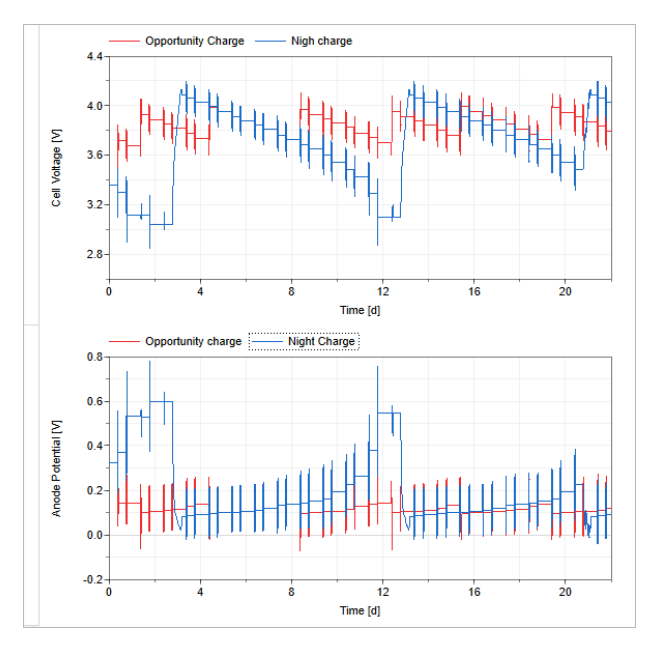


Figure 8. 4xWLTC per day, Gothenburg, lower heating temperature



**Figure 9.** Cell voltage and anode potential considering night and opportunity charge options

#### 5.2 Frequent charges at medium SOC

Finally, we present the results for the case in which the battery is allowed to recharge on-demand if the cell voltage drops below 3.6V, which leads to a lower DOD at lower SOC as in the previous case. As shown in Fig. 10, the opportunity charge can extend the life of the battery by over 400 days compared to night charge for the same SOH. This is so because the cell remains at a higher SOC for longer time than in the opportunity-charge strategy.

To minimize aging, as the literature indicates and we have seen in simulation, charging voltages and DOD should be selected as a function of the available charging locations and times, the daily usage, etc. We have discussed two cities with opposite climatic conditions. It is expected that locations with milder temperatures will require less energy for the thermal management (heater, chiller, etc.) and will result in intermediate SOH trajectories, assuming that the protection against plating is ensured.

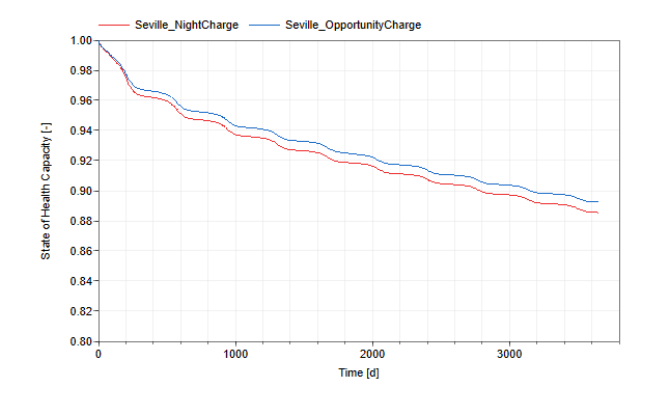


**Figure 10.** Remaining capacity results considering night and opportunity charge options

#### 6 Conclusions and future work

Aging of lithium ion batteries is a complex and challenging research area, and affects the safety and economics of electrification. This is of special importance in transportation electrification, where the multi-physics approach allows us to explore the effect of driving patterns, charging strategies, weather conditions and, more importantly, the particular aging dynamics of every cell chemistry.

Since full order electrochemical models with aging are computationally expensive and difficult to parameterize, we propose a reduced order model with SEI growth and lithium plating dynamics. The fitting effort is lower for the typical set of calendaric and cyclic tests, and conservative margins can be added to deal with parameter uncertainty and model limitations to better describe operational limits. As an example, we simulated different charging and thermal management strategies. Results show that lower temperatures and more frequent charging that reduce DOD and average SOC are beneficial, provided that anode potentials can be kept above the lithium plating onset.

Ongoing efforts are focused on improving the fidelity of the EHM, which involves an extension to cover electrolyte concentration dynamics (EHMe), as well as a P2D version with minimal discretization complexity to compare the influence of model inaccuracies. Additionally, experimental tests are currently being conducted to verify the simulated results presented.

# Acknowledgements

This work has been developed within DigiCell, a project funded by the European Union's Horizon research and innovation action under grant agreement No. 101135486.

#### References

Ali, Hayder et al. (2023). "Assessment of the calendar aging of lithium-ion batteries for a long-term—Space missions". In: *Frontiers in Energy Research* 11, p. 1108269.

Arora, P, RE White, and M Doyle (1998). "Capacity fade mechanisms and side reactions in lithium-ion batteries." In: *Journal of The Electrochemical Society* 145.10, pp. 3647–3667.

- Broussely, M (2002). "Aging Mechanisms and Calendar-Life Predictions in Lithium-Ion Batteries". In: *Advances in Lithium-Ion Batteries*. Ed. by WA van Schalkwijk and B Scrosati. 1st. New York: Springer US. Chap. 13, pp. 393–432.
- Broussely, M et al. (2001). "Aging mechanism in Li ion cells and calendar life predictions." In: *Journal of Power Sources* 97-98, pp. 13–21.
- Broussely, M. et al. (2005). "Main aging mechanisms in Li ion batteries". In: *Journal of Power Sources* 146.1-2, pp. 90–96.
- Chaturvedi, Nalin A et al. (2010). "Algorithms for advanced battery-management systems". In: *IEEE Control systems magazine* 30.3, pp. 49–68.
- Che, Yunhong et al. (2023). "Health prognostics for lithium-ion batteries: mechanisms, methods, and prospects". In: *Energy & Environmental Science* 16.2, pp. 338–371.
- Chen, Chang-Hui et al. (2020). "Development of experimental techniques for parameterization of multi-scale lithium-ion battery models". In: *Journal of The Electrochemical Society* 167.8, p. 080534.
- Christensen, John and John Newman (2006). "Stress generation and fracture in lithium insertion materials". In: *Journal of Solid State Electrochemistry* 10.5, pp. 293–319. arXiv: 0006334v1 [arXiv:cond-mat].
- Couto, Luis D. and Michel Kinnaert (2018). "Internal and Sensor Fault Detection and Isolation for Li-ion Batteries". In: *IFAC-PapersOnLine* 51.24, pp. 1431–1438.
- Couto, Luis D., Julien Schorsch, et al. (2016). "SOC and SOH estimation for Li-ion batteries based on an equivalent hydraulic model. Part I: SOC and surface concentration estimation". In: 2016 American Control Conference (ACC), pp. 4022–4028.
- Dao, Thanh-Son and Chad Schmitke (2015). "Developing Mathematical Models of Batteries in Modelica for Energy Storage Applications". In: *Proceedings of the 11th International Modelica Conference, Versailles, France, September 21-23, 2015.* 118. Linköping University Electronic Press, pp. 469–477.
- Doyle, Marc, Thomas F Fuller, and John Newman (1993). "Modeling of galvanostatic charge and discharge of the lithium/polymer/insertion cell". In: *Journal of the Electrochemical society* 140.6, p. 1526.
- Fu, Rujian et al. (2015). "Development of a physics-based degradation model for lithium ion polymer batteries considering side reactions". In: *Journal of Power Sources* 278, pp. 506–521.
- Goldar, Alejandro et al. (2020). "MPC strategies based on the equivalent hydraulic model for the fast charge of commercial Li-ion batteries". In: *Computers & Chemical Engineering* 141, p. 107010.
- Gu, WB and CY Wang (2000). "Thermal-electrochemical modeling of battery systems". In: *Journal of The Electrochemical Society* 147.8, p. 2910.
- Jin, Xing and Chang Liu (2019). "Physics-based controloriented reduced-order degradation model for LiNiMnCoO2 - graphite cell". In: *Electrochimica Acta* 312, pp. 188–201.
- Li, Yang et al. (2019). "Development of a degradation-conscious physics-based lithium-ion battery model for use in power system planning studies". In: *Applied Energy* 248, pp. 512–525.
- MapleSoft (2025). *MapleSim Battery Component Library*. https: //www.maplesoft.com/support/help/MapleSim/view.aspx? path = batteryComponentLibrary / Electrochem / LiIon & cid = 1778. Accessed: 2025-04-23.

- Otter, Martin, Karl-Erik Årzén, and Isolde Dressler (2005). "Stategraph-a modelica library for hierarchical state machines". In: *Modelica 2005 proceedings*. Halmstad University, pp. 569–578.
- Ploehn, HJ, P Ramadass, and RE White (2004). "Solvent Diffusion Model for Aging of Lithium-Ion Battery Cells." In: *Journal of The Electrochemical Society* 151.3, A456–A462.
- Rechkemmer, Sabrina Kathrin et al. (2019). "Empirical Li-ion aging model derived from single particle model". In: *Journal of Energy Storage* 21, pp. 773–786.
- Romagnoli, Raffaele et al. (2017). "Computationally-efficient constrained control of the state-of-charge of a li-ion battery cell". In: 2017 IEEE 56th Annual Conference on Decision and Control (CDC). IEEE, pp. 1433–1439.
- Romero, Alberto and Johannes Angerer (2023). "Fast Charge Algorithm Development for Battery Packs under Electrochemical and Thermal Constraints with JModelica. org". In: *Proceedings of the 15th International Modelica Conference, Aachen, Germany, 2023*, pp. 121–130.
- Romero, Alberto, Alejandro Goldar, Luis D. Couto, et al. (2019). "Fast charge of Li-ion batteries using a two-layer distributed MPC with electro-chemical and thermal constraints". In: *18th European Control Conference (ECC)*. IEEE, pp. 1796–1803.
- Romero, Alberto, Alejandro Goldar, and Emanuele Garone (2019). "A model predictive control application for a constrained fast charge of lithium-ion batteries". In: *Proceedings of the 13th International Modelica Conference, Regensburg, Germany, March 4–6, 2019.* 157. Linköping University Electronic Press.
- Schlasza, Christian et al. (2014). "Review on the aging mechanisms in Li-ion batteries for electric vehicles based on the FMEA method". In: 2014 IEEE Transportation Electrification Conference and Expo (ITEC). IEEE, pp. 1–6.
- Srinivasan, Venkat and CY Wang (2002). "Analysis of electrochemical and thermal behavior of Li-ion cells". In: *Journal of The Electrochemical Society* 150.1, A98.
- Vetter, J et al. (2005). "Ageing mechanisms in lithium-ion batteries". In: *Journal of Power Sources* 147.1-2, pp. 269–281.
- Wang, John et al. (2011). "Cycle-life model for graphite-LiFePO4 cells". In: *Journal of Power Sources* 196.8, pp. 3942–3948.
- Yang, Xiao-Guang, Yongjun Leng, et al. (2017). "Modeling of lithium plating induced aging of lithium-ion batteries: Transition from linear to nonlinear aging". In: *Journal of Power Sources* 360, pp. 28–40.
- Yang, Xiao-Guang and Chao-Yang Wang (2018). "Understanding the trilemma of fast charging, energy density and cycle life of lithium-ion batteries". In: *Journal of Power Sources* 402, pp. 489–498.
- Zhao, Yinyin, Song-Yul Choe, and Jungdo Kee (2018). "Modeling of degradation effects and its integration into electrochemical reduced order model for Li(MnNiCo)O2/Graphite polymer battery for real time applications". In: *Electrochimica Acta* 270, pp. 440–452.